Finite Elements in Analysis and Design (Re-submitted in November 2004)

Accurate Determination of Mode I and II Leading Coefficients of the Williams Expansion by Finite Element Analysis

R.K.L. Su[a,*] and W.J. Feng[b]

[a] Department of Civil Engineering, The University of Hong Kong, Pokfulam Road, Hong Kong, PRC, email address: klsu@hkucc.hku.hk

[b] Department of Mechanics and Engineering Science, Shijiazhuang Railway Institute, Shijiazhuang 050043, PRC, email address: fengwj@sjzri.edu.cn

* corresponding author

Abstract

Leading coefficients of the Williams expansion are evaluated by using the fractal finite element method (FFEM). By means of the self-similarity principle, an infinite number of elements is generated at the vicinity of the crack tip to model the crack tip singularity. The Williams expansion series with higher-degree coefficients is used to capture the singular

and non-singular stress behaviour around the crack tip and to condense the large amount of nodal displacements at the crack tip to a small set of unknown coefficients. New sets of coefficients up to the sixth degree for mode I and the fourth degree for mode II problems are solved. The important fracture parameters such as stress intensity factors and *T*-stress can be obtained directly from the coefficients without employing any path independent integrals. Convergence study reveals that the present method is simple and very coarse finite element meshes with 12 leading terms in the William expansion can yield very accurate solutions. The effects of the influence of crack length on the higher-degree coefficients of some common plane crack problems are studied in detail.

Keywords: fractal finite element, stress intensity factor, *T*-stress, higher-degree coefficients, Williams expansion

1. Introduction

Assuming plane crack with traction-free faces subjected to arbitrary remote loading, the linear elastic displacement and stress fields at the crack tip obtained by the Williams eigenfunction expansion technique [1] can be expressed as,

$$v_x = \sum_{n=0}^{\infty} \frac{r^{n/2}}{2\mu} \left\{ a_n \left[\left(\kappa + \frac{n}{2} + (-1)^n \right) \cos\frac{n}{2}\theta - \frac{n}{2}\cos\left(\frac{n-4}{2} \right)\theta \right] - b_n \left[\left(\kappa + \frac{n}{2} - (-1)^n \right) \sin\frac{n}{2}\theta - \frac{n}{2}\sin\left(\frac{n-4}{2} \right)\theta \right] \right\} \tag{1}$$

$$v_y = \sum_{n=0}^{\infty} \frac{r^{n/2}}{2\mu} \left\{ a_n \left[\left(\kappa - \frac{n}{2} - (-1)^n \right) \sin\frac{n}{2}\theta + \frac{n}{2} \sin\left(\frac{n-4}{2} \right)\theta \right] + b_n \left[\left(\kappa - \frac{n}{2} + (-1)^n \right) \cos\frac{n}{2}\theta + \frac{n}{2} \cos\left(\frac{n-4}{2} \right)\theta \right] \right\} \quad (2)$$

$$\sigma_x = \sum_{n=1}^{\infty} \frac{n}{2} r^{(n/2-1)} \left\{ a_n \left[\left(2 + \frac{n}{2} + (-1)^n \right) \cos\left(\frac{n}{2} - 1 \right)\theta - \left(\frac{n}{2} - 1 \right) \cos\left(\frac{n}{2} - 3 \right)\theta \right] - b_n \left[\left(2 + \frac{n}{2} - (-1)^n \right) \sin\left(\frac{n}{2} - 1 \right)\theta - \left(\frac{n}{2} - 1 \right) \sin\left(\frac{n}{2} - 3 \right)\theta \right] \right\} \quad (3)$$

$$\sigma_y = \sum_{n=1}^{\infty} \frac{n}{2} r^{(n/2-1)} \left\{ a_n \left[\left(2 - \frac{n}{2} - (-1)^n \right) \cos\left(\frac{n}{2} - 1 \right)\theta + \left(\frac{n}{2} - 1 \right) \cos\left(\frac{n}{2} - 3 \right)\theta \right] - b_n \left[\left(2 - \frac{n}{2} + (-1)^n \right) \sin\left(\frac{n}{2} - 1 \right)\theta + \left(\frac{n}{2} - 1 \right) \sin\left(\frac{n}{2} - 3 \right)\theta \right] \right\} \quad (4)$$

$$\tau = \sum_{n=1}^{\infty} \frac{n}{2} r^{(n/2-1)} \left\{ a_n \left[\left(\frac{n}{2} - 1 \right) \sin\left(\frac{n}{2} - 3 \right)\theta - \left(\frac{n}{2} + (-1)^n \right) \sin\left(\frac{n}{2} - 1 \right)\theta \right] + b_n \left[\left(\frac{n}{2} - 1 \right) \cos\left(\frac{n}{2} - 3 \right)\theta - \left(\frac{n}{2} - (-1)^n \right) \cos\left(\frac{n}{2} - 1 \right)\theta \right] \right\}. \quad (5)$$

where r and θ are the polar coordinates, μ is the shear modulus, ν is Poisson's ratio, $\kappa = (3-4\nu)$ for plane strain condition and $(3-\nu)/(1+\nu)$ for plane stress condition and n is the degree of term in the infinite series. It is well known that the first degree coefficients (a_1 and b_1) in the series is directly associated with the singular stress behaviour and can be related to stress intensity factors which are primarily important in prediction of crack initiation and propagation in brittle materials. The first non-singular stress term (n=2) which acts parallel to the crack at its tip, of the Williams eigenfunction expansion series [1] is known as T-stress which can be related to the coefficient a_2. The experimental results on

mixed mode loads [2 & 3] showed that the inclusion of this term of the stress distribution could produce an improved correlation with fracture predictions for the angle of fracture and the critical stress intensity factor. Furthermore, *T*-stress was found to have significant effects on fracture toughness [4], size and shape of the crack-tip plastic zone [5 & 6] and stability of the crack path direction [7-10]. The application of both the stress intensity factor and the *T*-stress to include the constraint effect in failure investigations is becoming increasingly popular [11]. Further investigations on the second non-singular term (n=3) found that it has significant effect on the centre-cracked and single-edge specimens with short crack lengths [12] and it has smaller effect than that of the *T*-stress on the variation of apparent fracture toughness in brittle materials [13].

It is therefore important to obtain the leading coefficients of the Williams expansion for the cracked geometries under consideration. Several analytical and numerical methods have been developed to evaluate the stress intensity factor and *T*-stress for the cracked configurations [14-22] but not the higher-degree coefficients. While only Karihaloo and Xiao [14] recently developed a higher order hybrid crack element to evaluate the higher-degree solutions. They found that accurate determination of the higher-degree coefficients was more difficult than that of the stress intensity factors; and it requires higher order hybrid crack elements together with a finer subdivision of the remainder of the body by regular elements. The hybrid crack element method had been applied to determine the higher-degree coefficients for the standard compact tension specimen [23] and wedge splitting specimens [24]. So far only mode I solutions, up to n=5, have been evaluated.

In this paper, an alternative technique namely the fractal finite element method (FFEM), which has been proven to be an accurate and efficient method to solve planar crack problems [25-27], is employed to determine the higher-degree coefficients. Numerical examples are given and compared with previous results to demonstrate the convergence, efficiency and accuracy of the present approach. Accurate leading coefficients for mode I and II problems are evaluated. The results indicate that the present method is simple; and do not require matrix inversion to formulate the element stiffness matrices or any post-processing technique to obtain the coefficients. It is also found that relatively coarse finite element mesh with 12 terms of the Williams expansion is sufficient to yield very accurate leading coefficients.

2. Brief Formulation of the Fractal Finite Element Method

The FFEM was originated in 1993 by Leung and Su to handle crack related problems [25]. This method was modified from the two-level finite element method (2LFEM) [28] of which the principle was that, while the local interpolating shape function could reduce infinite number of degrees of freedom (DOF) within a finite element to finite number of nodal displacements, the global interpolation function (Williams expansion with higher-degree terms) could further reduce the nodal displacements to a small set of unknown coefficients. The FFEM extends this concept by generating self-similar meshes at the crack tip region (see Fig. 1) with infinite number of nodal DOF around the singular point. By using the fractal transformation [27], an infinite nodal DOF is condensed expeditiously

without increasing the order of the final equations as well as the computational time. The stress intensity factors and *T*-stress can be obtained directly from those coefficients.

The FFEM has been used to determinate stress intensity factors and *T*-stress, it is the first time to extend this method to calculate the leading coefficients of mode I and mode II crack problems. For completeness, brief formulation of the FFEM is presented. To simplify our discussion, typical 9-node isoparametric elements with two DOF per node will be used to illustrate the formulation of the FFEM. However, similar theory can be applied to elements with different node numbers and different formulations.

Based on conventional finite element methods [29], the first level interpolation in a finite element (say the l^{th} element) is achieved by using the conventional shape function $\hat{\mathbf{N}}$,

$$\hat{\mathbf{u}}_{2\times1} = \hat{\mathbf{N}}_{2\times18}\hat{\mathbf{d}}_{18\times1} \tag{6}$$

where $\hat{\mathbf{u}} = \{\hat{u}_x \quad \hat{u}_y\}^T$ is the displacement vector in the l^{th} element and $\hat{\mathbf{d}} = \{\cdots \quad \hat{v}_x^k \quad \hat{v}_y^k \quad \cdots\}^T$ is the nodal displacement vector. The symbol '$\wedge$' used here is to denote the vector or matrix in element level. Furthermore, considering the nodal displacement $\hat{\mathbf{v}}^k = \{\hat{v}_x^k \quad \hat{v}_y^k\}^T$ at the k^{th} node of the element, the displacement can be represented by the global interpolation. Hence,

$$\hat{\mathbf{v}}^k{}_{2\times1} = \hat{\mathbf{T}}^k{}_{2\times2(N+1)}\bar{\mathbf{a}}_{2(N+1)\times1} \tag{7}$$

where $\bar{\mathbf{a}} = \{a_0 \quad b_0 \quad a_1 \quad b_1 \quad a_2 \quad b_2 \quad \cdots\}^T$ is the unknown coefficient vector of the Williams eigenfunction series. The superscript '-' denotes the vector or matrix of the fractal mesh in inter-element level. The first two coefficients a_0 and b_0 are associated with

the rigid body motions at the crack tip of the fractal mesh. It is not difficult to observe that the second-degree stress functions corresponding to b_2 in equations (3) to (5) are always equal to zero. Therefore the coefficient b_2 is arbitrary and may be taken as zero for simplicity. The explicit form of the global interpolation function $\hat{\mathbf{T}}^k$ can be expressed as,

$$\hat{\mathbf{T}}^k = \frac{1}{2\mu}\begin{bmatrix} 1 & 0 & \cdots & r^{\frac{n}{2}}\left[\left(\kappa+\frac{n}{2}+(-1)^n\right)\cos\frac{n\theta}{2}-\frac{n}{2}\cos\left(\frac{n-4}{2}\right)\theta\right] \\ 0 & 1 & \cdots & r^{\frac{n}{2}}\left[\left(\kappa-\frac{n}{2}-(-1)^n\right)\sin\frac{n\theta}{2}+\frac{n}{2}\sin\left(\frac{n-4}{2}\right)\theta\right] \\ & & & -r^{\frac{n}{2}}\left[\left(\kappa+\frac{n}{2}-(-1)^n\right)\sin\frac{n\theta}{2}-\frac{n}{2}\sin\left(\frac{n-4}{2}\right)\theta\right] \quad \cdots \\ & & & r^{\frac{n}{2}}\left[\left(\kappa-\frac{n}{2}+(-1)^n\right)\cos\frac{n\theta}{2}+\frac{n}{2}\cos\left(\frac{n-4}{2}\right)\theta\right] \quad \cdots \end{bmatrix} \quad n=1\ldots N \tag{8}$$

It is noted that usually large amount of conventional finite elements is required to simulate the singularity at the crack tip. The order of nodal displacement vector in the singular region is in general much larger than that of $\bar{\mathbf{a}}$. When infinite number of self-similar layers of elements is generated around the crack tip (as shown in Fig. 1) which leads to infinite number of unknown displacements, the transformation equation (7) can be used to condense the associated infinite number of DOF to a finite number of unknown coefficients $\bar{\mathbf{a}}$.

To perform the transformation, the elements on the first layer and the inner layers of the fractal mesh have to be considered separately. For the first layer of the fractal mesh, let there is M number of master nodes on the boundary Γ_0 as shown in Fig. 1. The displacement vector associated with the master nodes is denoted as $\{\hat{\mathbf{d}}_m\}_{2M\times 1}$. The displacement vector within the boundary Γ_0 corresponding to the slave nodes is

represented by $\{\hat{\mathbf{d}}_s\}_{(18-2M)\times 1}$. To carry out the transformation, the element stiffness matrix $\hat{\mathbf{K}}^f$ of the first layer of mesh is first partitioned with respect to *s* and *m*,

$$\hat{\mathbf{K}}^f_{18\times 18}\hat{\mathbf{d}}_{18\times 1} = \begin{bmatrix} \hat{\mathbf{K}}^f_{ss} & \hat{\mathbf{K}}^f_{sm} \\ \hat{\mathbf{K}}^f_{ms} & \hat{\mathbf{K}}^f_{mm} \end{bmatrix} \begin{Bmatrix} \hat{\mathbf{d}}_s \\ \hat{\mathbf{d}}_m \end{Bmatrix} \tag{9}$$

where the superscript *f* indicates the first layer of the fractal mesh. Only the displacements at the slaves are transformed. The second level (global) interpolation of displacements can be written as follows,

$$\begin{Bmatrix} \hat{\mathbf{d}}_s \\ \hat{\mathbf{d}}_m \end{Bmatrix}_{18\times 1} = \begin{bmatrix} \hat{\mathbf{T}}^f_{(18-2M)\times 2(N+1)} & \\ & \mathbf{I}_{2M\times 2M} \end{bmatrix} \begin{Bmatrix} \bar{\mathbf{a}} \\ \hat{\mathbf{d}}_m \end{Bmatrix}_{[2+2N+2M]\times 1} \tag{10}$$

Where $\mathbf{I}$ is the identity matrix and $\hat{\mathbf{T}}^f = \begin{Bmatrix} \cdots & \hat{\mathbf{T}}^k & \cdots \end{Bmatrix}^T$ is the transformation matrix that can be obtained from equation (8). After transforming the stiffness matrix of the l^{th} element on the first layer of the fractal mesh, one has,

$$\hat{\mathbf{K}}^f_{(2+2N+2M)\times(2+2N+2M)} = \begin{bmatrix} \hat{\mathbf{T}}^{f\,T}\hat{\mathbf{K}}^f_{ss}\hat{\mathbf{T}}^f & \hat{\mathbf{T}}^{f\,T}\hat{\mathbf{K}}^f_{sm} \\ sys & \hat{\mathbf{K}}^f_{mm} \end{bmatrix} \tag{11}$$

For the inner elements located in the same sector of the l^{th} element (see Fig. 2), all the DOF is transformed to the unknown coefficients. Due to geometric self-similarity between successive layers of the fractal mesh, a simple geometric progression relationship known as fractal transformation [27] was found for transforming and assembling all the inner layer elements, such that,

$$\hat{\mathbf{K}}^i_{(2+2N)\times(2+2N)} = \begin{bmatrix} & \vdots & \\ \cdots & \alpha_{ij}\hat{k}^f_{ij} & \cdots \\ & \vdots & \end{bmatrix} \tag{12}$$

$$\alpha_{ij} = \begin{cases} 1 & \text{when } i_1 = 0 \text{ or } j_1 = 0 \\ \dfrac{1}{\left(2^{(i_1+j_1)}-1\right)} & \text{else} \end{cases} \quad ; i_1 = Int\left(\frac{i-1}{2}\right) \text{ and } j_1 = Int\left(\frac{j-1}{2}\right) \tag{13}$$

$\hat{k}_{ij}^{f}$ is the ij^{th} entry in $\left[\hat{\mathbf{T}}^{f}\right]^{T}_{2(N+1)\times 18}\left[\hat{\mathbf{K}}^{f}\right]_{18\times 18}\left[\hat{\mathbf{T}}^{f}\right]_{18\times 2(N+1)}$ (14)

The generalized stiffness matrix $\hat{\mathbf{K}}_s$ of that sector can then be expressed as,

$$\hat{\mathbf{K}}_s \begin{Bmatrix} \overline{\mathbf{a}} \\ \hat{\mathbf{d}}_m \end{Bmatrix} = \begin{bmatrix} \hat{\mathbf{K}}^{f} + \hat{\mathbf{K}}^{i} & \hat{\mathbf{T}}^{f\,T}\hat{\mathbf{K}}^{f}_{sm} \\ sys & \hat{\mathbf{K}}^{f}_{mm} \end{bmatrix} \begin{Bmatrix} \overline{\mathbf{a}} \\ \hat{\mathbf{d}}_m \end{Bmatrix} \tag{15}$$

So far, only a sector of the elements along the perimeter Γ, as shown in Fig. 2, is transformed. The global generalized stiffness matrix $\overline{\mathbf{K}}_s$ for the fractal mesh can be calculated by summing up the generalized stiffness matrix $\hat{\mathbf{K}}_s$ associated with all the sectors, hence,

$$\overline{\mathbf{K}}_s \begin{Bmatrix} \overline{\mathbf{a}} \\ \overline{\mathbf{d}}_m \end{Bmatrix} = \left[\sum_{the\ \mathrm{sec}tor} \hat{\mathbf{K}}_s \right] \begin{Bmatrix} \overline{\mathbf{a}} \\ \overline{\mathbf{d}}_m \end{Bmatrix} \tag{16}$$

By means of the master nodes, the singular region can be merged with the regular region which is modelled by the conventional finite elements as shown in Fig. 1. All the coefficients in equation (16) can be solved after applying the appropriate boundary conditions.

Invoking the definitions of the stress intensity factors and the *T*-stress, those fracture parameters can be related to the coefficients as,

$$K_I = a_1\sqrt{2\pi}\ , \quad K_{II} = -b_1\sqrt{2\pi} \text{ and } T = 4a_2 \tag{17}$$

3.0 Test of Convergence

It has been mentioned [14] that accurate determination of the higher-degree coefficients by finite element analysis was more difficult than that of the stress intensity factors; and it requires more terms in the Williams expansion together with a finer subdivision of the remainder of the body by regular elements. Similar convergence study for the FFEM had been performed [30] and suggested using full Gaussian integration scheme to evaluate the nine-node Lagrangian element and circular fractal meshes c4 to model a quarter or half of the cracked regions. However that study only focused on the accurate determination of the stress intensity factors (the first term, n=1 in the series) but not the other higher-degree terms. As motivated by the study of Karihaloo and Xiao [14], test of convergence for the higher-degree terms is conducted and the influences of the density of fractal mesh and the number of terms used in the Williams expansion are studied.

Figure 3 shows two specimens, single edge crack in tension (SECT) and single edge crack in shear (SECS). The width (W) and height ($2H$) of the two specimens are the same and both equal to 4 units (H=W=4). The crack length a for SECT and SECS specimens are chosen as 1 and 2 units, respectively. The material properties are selected as E=20000 and ν=0.3. Due to symmetry, only half of the plate is modelled. Two finite element meshes, c4 (with 4 fractal elements in each layer of fractal mesh) and c8 (with 8 fractal elements in each layer of fractal mesh) as shown in Fig. 4 are constructed to check the accuracy of the solutions.

The numerical results of the higher-degree coefficients for SECT had been presented in reference [14]. The highest term used in the Williams expansion is N=12 in the FFEM. Table 1 shows a comparison of the present results with those available from the literatures. Fractal mesh c4 can accurately predict up to n=3 of the coefficients for the mode I crack, whereas fractal mesh c8 can give accurate results up to n=5. The results obtained from c4 mesh are consistent with that of c8 up to n=3 and n=2 for mode I and mode II problems respectively. This finding also supported by Karihaloo and Xiao [14] that finer subdivision of finite element mesh is required to achieve high accuracy in higher-degree term calculation. By using c8 mesh, the present results and those available in the literatures are generally agreed with less than 2% differences.

The convergence of the higher-degree coefficients with the total number of terms (N) in the Williams expansion is studied. By using c8 mesh, the higher-degree coefficients up to n=6 for the problems of SECT and SECS are calculated and the results are shown in Figure 5. It can be seen that all the coefficients converged steadily with increasing value of N for SECT. In general N=12 is sufficient for achieving less than 1% discrepancy with the converged value for mode I problems. For mode II problems, the 4^{th}- and lower-degree coefficients converge rapidly when N >11. However, the 5^{th} and higher-degree coefficients do not converge steadily for more than 20 terms in the truncated Williams expansion. The higher-degree coefficients for mode II problems are much more difficult to determine than that of mode I problems.

4.0 Numerical Examples

To demonstrate the efficiency and accuracy of the present method, leading coefficients are calculated for five typical problems as shown in Figure 6. In these examples, the models are defined as H=W=4, Poisson's ratio ν=0.3 and Young's modulus E =20000. The crack length to width ratio (a/W) is varied from 0.1 to 0.7. Under symmetry conditions, only half or a quarter of the plates is needed in the analyses. By using c8 fractal mesh and 12 terms in the truncated Williams expansion series, the results for the leading coefficients up to n=6 and n=4 for Mode I and Mode II problems are calculated and shown in Tables 2 and 3 respectively. The results are compared with the previous available stress intensity factor solutions derived by the finite strip approach [31]. For all the cases, excellent agreement with less than 1% differences is observed.

5.0 Conclusions

By using the fractal finite element method, the leading coefficients of the Williams expansion of various crack configurations have been evaluated. The present method has been shown to be relatively simple to implement, as no new element formulation and no post-processing technique are required for determination of the higher-degree coefficients. Convergence study reveals that finer fractal meshes have to be used to get accurate higher-degree coefficients. Fractal mesh c8 together with 12 transformation terms is sufficient to yield coefficients with less than 2% discrepancy between the present and the available literature results of leading coefficients up to n=6 for mode I crack problems. However, the higher-degree coefficients ($n\geq5$) for mode II problems are difficult to accurately determine. The effects of the influence of crack length on the higher-degree coefficients, up to n=6 for mode I and n=4 for mode II, of some common plane crack problems are presented.

Acknowledgements

The work described in this paper was fully supported by the grant from the Committee on Research and Conference Grants (CRCG) through small project funding 2004-05, The University of Hong Kong.

References

[1] M.L. Williams, On the Stress Distribution at the Base of a Stationary Crack, ASME Journal of Applied Mechanics 24 (1957) 109-114.

[2] J.G. Williams, P.D. Ewing, Fracture under Complex Stress – the Angled Crack Problem, International Journal of Fracture Mechanics 8 (1972) 441-446.

[3] Y. Ueda, K. Ikeda, T. Yao, Characteristics of Brittle Fracture under General Combined Modes including those under Bi-axial Tensile Loads, Engineering Fracture Mechanics 18 (1983) 1131-1158.

[4] D.J. Smith, M.R. Ayatollahi, M.J. Pavier, The Role of T-stress in Brittle Fracture for Linear Elastic Materials under Mixed-Mode Loading, Fatigue & Fracture of Engineering Materials & Structures 24 (2001) 137-150.

[5] S.G. Larsson, A.J. Carlsson, Influence of Non-Singular Stress Terms and Specimen Geometry on Small-Scale Yielding at Crack-Tips in Elastic-Plastic Materials, Journal of the Mechanics and Physics of Solids 21 (1973) 263-277.

[6] J.R. Rice, Limitations to the Small Scale Yielding Approximation for Crack Tip Plasticity, Journal of the Mechanics and Physics of Solids 22 (1974) 17-26.

[7] B. Cotterell, J.R. Rice, Slightly Curved or Kinked Cracks, International Journal of Fracture 16 (1980) 155-169.

[8] B.L. Karihaloo, L.M. Keer, S. Nemat-Nasser, A. Oranratnachai, Approximate Description of Crack Kinking and Curving, Journal of Applied Mechanics –Transactions of the ASME 48 (1981) 515-519.

[9] S. Melin, The Influence of the T-stress on the Directional Stability of Cracks, International Journal of Fracture 114 (2002) 259-265.

[10] T. Fett, D. Munz, T-Stress and Crack Path Stability of DCDC Specimens, International Journal of Fracture 124 (2003) L165-L170.

[11] A.H. Sherry, C.C. France, M.R. Goldthorpe, Compendium of T-stress Solutions for Two and Three-Dimensional Cracked Geometries, Fatigue & fracture of engineering materials & structures 18 (1995) 141-155.

[12] G.A. Kardomateas, R.L. Carlson, A.H. Soediono, D.P. Schrage, Near-Tip Stress and Strain Fields for Short Elastic Cracks, International Journal of Fracture 62, (1993) 219-232.

[13] Y.J. Chao, X.H. Zhang, Constraint Effect in Brittle Fracture, Proceedings of the 1995 27th International Symposium on Fatigue and Fracture Mechanics, ASTM STP 1296, American Society for Testing and Materials, Philadelphia, PA, 1997, p. 41-60.

[14] B.L. Karihaloo, Q.Z. Xiao, Accurate Determination of the Coefficients of Elastic Crack Tip Asymptotic Field by a Hybrid Crack Element with p-Adaptivity, Engineering Fracture Mechanics 68 (2001), 1609-1630.

[15] T. Fett. A Compendium of T-stress Solutions. Report FZKA 6057, Forschungs-zentrum Karlsruhe, 1998.

[16] C.L. Tan, X. Wang, The Use of Quarter-Point Crack Tip Elements for T-stress Determination in Boundary Element Method Analysis, Engineering Fracture Mechanics 70 (2003) 2247-2252.

[17] C.S. Chen, R. Krause, R.G. Pettit, L. Banks-Sills, A.R. Ingraffea, Numerical Assessment of T-stress Computation using a p-Version Finite Element Method, International Journal of Fracture 107(2001) 177-199.

[18] P.S. Leevers, J.C. Radon, Inherent Stress Biaxiality in Various Fracture Specimen Geometries, International Journal of Fracture 19 (1982) 311-325.

[19] G.E. Cardew, M.R. Goldthorpe, I.C. Howard, A.P. Kfouri, On the Elastic T-term, In: Bilby BA, Miller KJ and Willis JR editors, Fundamentals of Deformation and Fracture, Cambridge University Press, Cambridge, 1984.

[20] A.P. Kfouri, Some Evaluations of the Elastic T-term Using Eshelby's Method, International Journal of Fracture 30(1986) 301-315.

[21] J.D. Eshelby, The Calculation of Energy Release Rates, In: Sih GC, van Elst HC, Broek D, editors. Prospects of fracture mechanics. Noordhoff International, 1975.

[22] T.L. Sham, The Determination of the Elastic T-term Using Higher Order Weight Functions, International Journal of Fracture 48 (1991) 81-102.

[23] Q.Z. Xiao, B.L. Karihaloo, Coefficients of the Crack Tip Asymptotic Field for a Standard Compact Tension Specimen, International Journal of Fracture 118(2002) 1-15.

[24] B.L. Karihaloo, H. Abdalla, Q.Z. Xiao, Coefficients of the Crack Tip Asymptotic Field for Wedge Splitting Specimens, Engineering Fracture Mechanics 70 (2003) 2407-2420.

[25] A.Y.T. Leung, R.K.L. Su, Fractal Two-Level Finite Element Methods for 2-D Crack Problems, Proceedings of the Second Asian-Pacific Conference on Computational Mechanics, Sydney Australia, 1993, pp675-679.

[26] A.Y.T. Leung, R.K.L. Su, Mode I Crack Problems by Fractal Two-Level Finite Element Methods, Engineering Fracture Mechanics 48(1994) 847-856.

[27] A.Y.T. Leung, R.K.L. Su, Mixed Mode Two-Dimensional Crack Problems by Fractal Two-Level Finite Element Method, Engineering Fracture Mechanics 51(1995) 889-895.

[28] A.Y.T. Leung, S.C. Wong, Two-Level Finite Element Method for Plane Cracks, Communications in Applied Numerical Methods 5 (1989) 263-274.

[29] R.D. Cook, D.S. Malkus, M.E. Plesha, Concepts and Applications of Finite Element Analysis, 3rd Edition. John Wiley & Son: New York, 1989.

[30] A.Y.T. Leung, R.K.L. Su, Fractal Two-Level Finite Element Method for Two-Dimensional Cracks, Microcomputers in Civil Engineering 11(1996) 249-257.

[31] Y.K. Cheung, C.P. Jiang, Application of the Finite Strip Method to Plane Fracture Problems, Engineering Fracture Mechanics 53 (1996) 89-96.

Table 1. Comparison of the higher-degree coefficients: H/W=1 and N=12.

SECT (a/W=0.25)			
Coefficients	Ref[14]	FFEM-c4	FFEM-c8
a_1	1.0585	1.0592 (0.7%)	1.0593 (0.1%)
a_2	-0.1513	-0.1513 (0%)	-0.1506 (-0.5%)
a_3	0.0815	0.0801 (-1.7%)	0.0796 (-2.3%)
a_4	-0.0478	-0.0441* (-7.7%)	-0.0476 (-0.4%)
a_5	0.0055	0.0093* (69%)	0.0054 (-1.8%)
SECS (a/W=0.5)			
Coefficients	Ref[31]	FFEM-c4	FFEM-c8
b_1	-0.4789	-0.4654(-2.8%)	-0.4804(0.3%)
b_2		0.0000	0.0000
b_3		0.0560*	0.0871
b_4		0.0603*	-0.0414
b_5		-0.0239*	-0.0156*

value in the bracket represents the percentage differences with the references

* not accurate

Table 2. Variations of the higher-degree coefficients for mode I problems
(H/W=1 and N=12)

a/W	a_1 Ref[31]	a_1	a_2	a_3	a_4	a_5	a_6
SECT							
0.1		0.5318	-0.1376	0.1837	-0.1244	0.0613	0.1220
0.2		0.8649	-0.1472	0.1143	-0.0622	0.0156	0.0347
0.3		1.2863	-0.1519	0.0355	-0.0360	-0.0033	0.0180
0.4		1.8892	-0.1427	-0.1087	-0.0136	-0.0258	0.0142
0.5	2.834	2.8247	-0.1025	-0.4117	0.0201	-0.0737	0.0202
0.6		4.4169	0.0127	-1.1260	0.0976	-0.2099	0.0512
0.7		7.5169	0.3425	-3.1306	0.3432	-0.7105	0.1925
CCT							
0.1		0.4533	-0.2547	0.2833	0.0001	-0.0886	-0.0005
0.2		0.6673	-0.2681	0.2061	0.0016	-0.0348	0.0004
0.3		0.8698	-0.2888	0.1713	0.0049	-0.0247	0.0010
0.4		1.0874	-0.3149	0.1438	0.0102	-0.0245	0.0013
0.5	1.338	1.3333	-0.3462	0.1130	0.0163	-0.0289	0.0012
0.6		1.6216	-0.3872	0.0751	0.0202	-0.0378	0.0012
0.7		1.9838	-0.4567	0.0306	0.0146	-0.0599	0.0041
DECT							
0.1		0.5084	-0.1330	0.1821	-0.1214	0.0619	0.1172
0.2		0.7446	-0.1341	0.1269	-0.0581	0.0184	0.0316
0.3		0.9528	-0.1283	0.0922	-0.0312	0.0050	0.0153
0.4		1.1480	-0.1104	0.0594	-0.0121	-0.0008	0.0088
0.5	1.333	1.3326	-0.0793	0.0298	0.0025	-0.0007	0.0046
0.6		1.5167	-0.0384	0.0132	0.0124	0.0063	0.0010
0.7		1.7340	0.0055	0.0277	0.0167	0.0242	-0.0024

Table 3. Variations of the higher-degree coefficients for mode II problems (H/W=1 and N=12)

a/W	b_1 Ref[31]	b_1	b_3	b_4
SECS				
0.1		-0.9149	1.1861	-0.6876
0.2		-0.6529	0.4202	-0.1764
0.3		-0.5464	0.2176	-0.0858
0.4		-0.4965	0.1352	-0.0505
0.5	-0.4789	-0.4803	0.0871	-0.0414
0.6		-0.4936	0.0573	-0.0508
0.7		-0.5435	0.0349	-0.0774
CCS				
0.1		-0.3596	0.3649	-0.0132
0.2		-0.2669	0.1274	-0.0070
0.3		-0.2348	0.0656	-0.0064
0.4		-0.2242	0.0412	-0.0081
0.5	-0.2260	-0.2263	0.0272	-0.0107
0.6		-0.2401	0.0185	-0.0173
0.7		-0.2692	0.0128	-0.0334

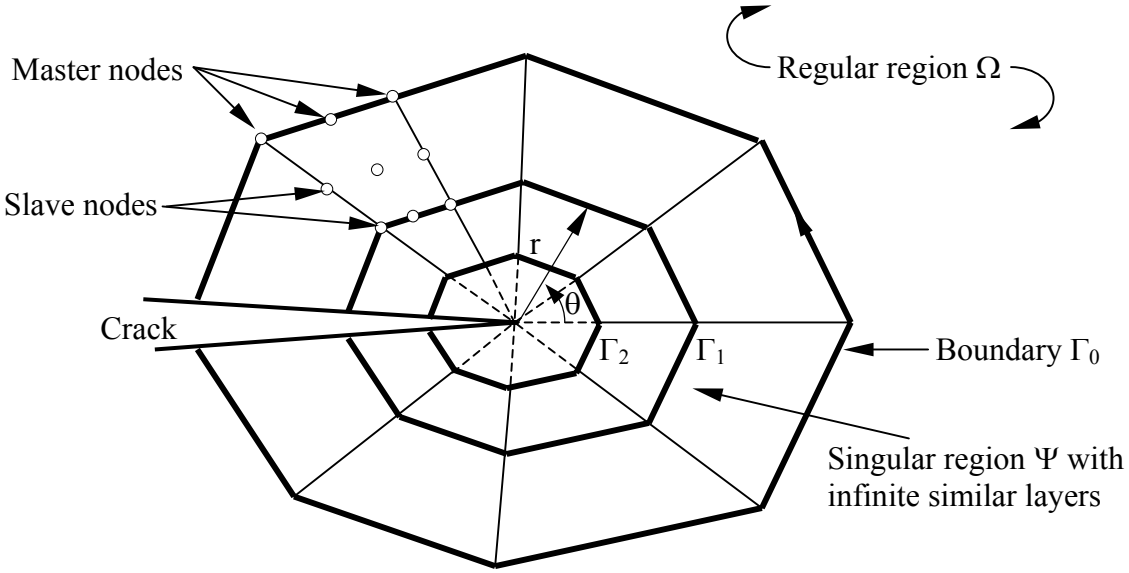

Fig. 1. Regular and singular regions and construction of fractal mesh.

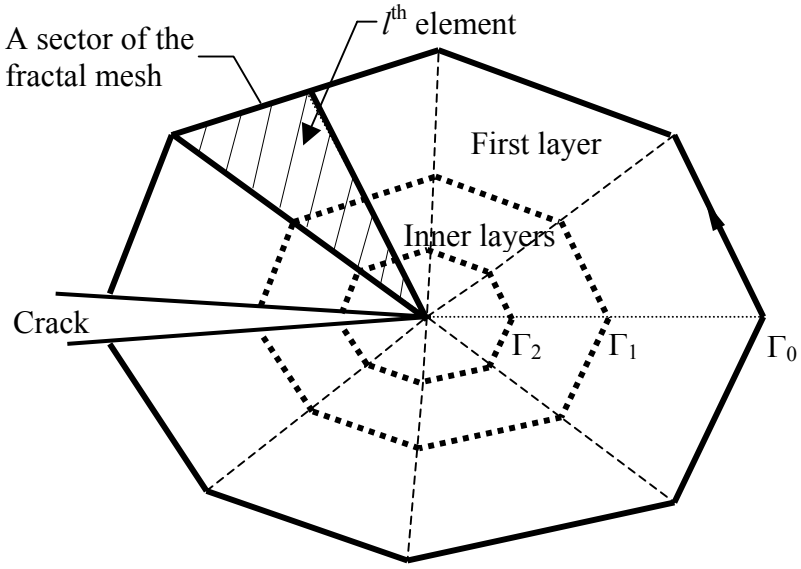

Fig. 2. A sector in the fractal mesh.

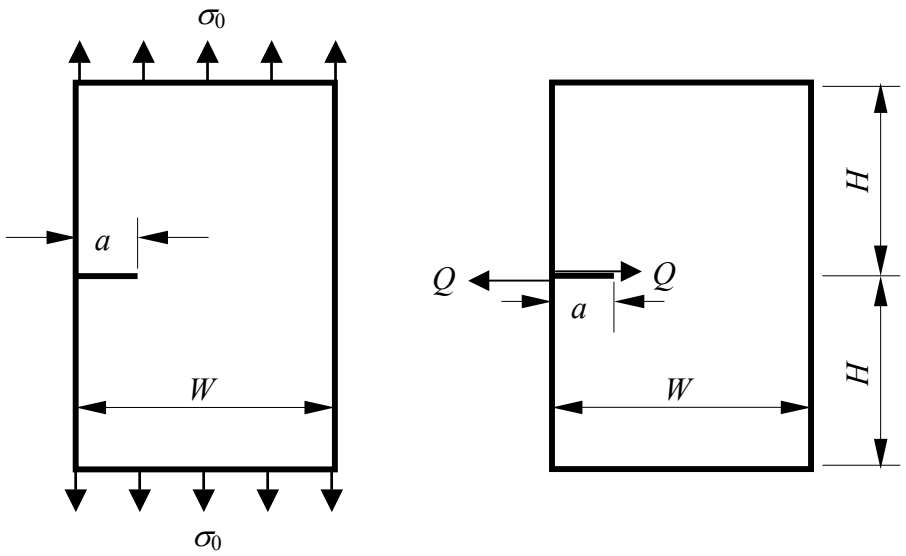

(a) SECT (b) SECS

Fig. 3. Example problems for convergence study of the higher-degree coefficients: (a) Single Edge Crack Tension (SECT) and (b) Single Edge Crack Shear (SECS). (H=W=4)

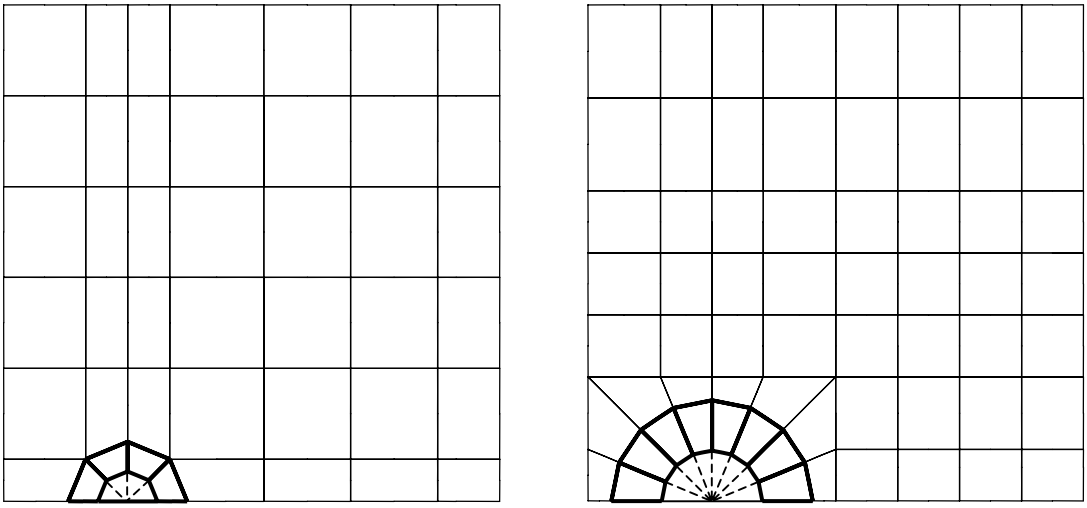

(a) c4
number of elements=44
number of nodes=208

(b) c8
number of elements=64
number of nodes=296

Fig. 4. Fractal mesh configurations: (a) c4 and (b) c8. (*a/W*=0.25)

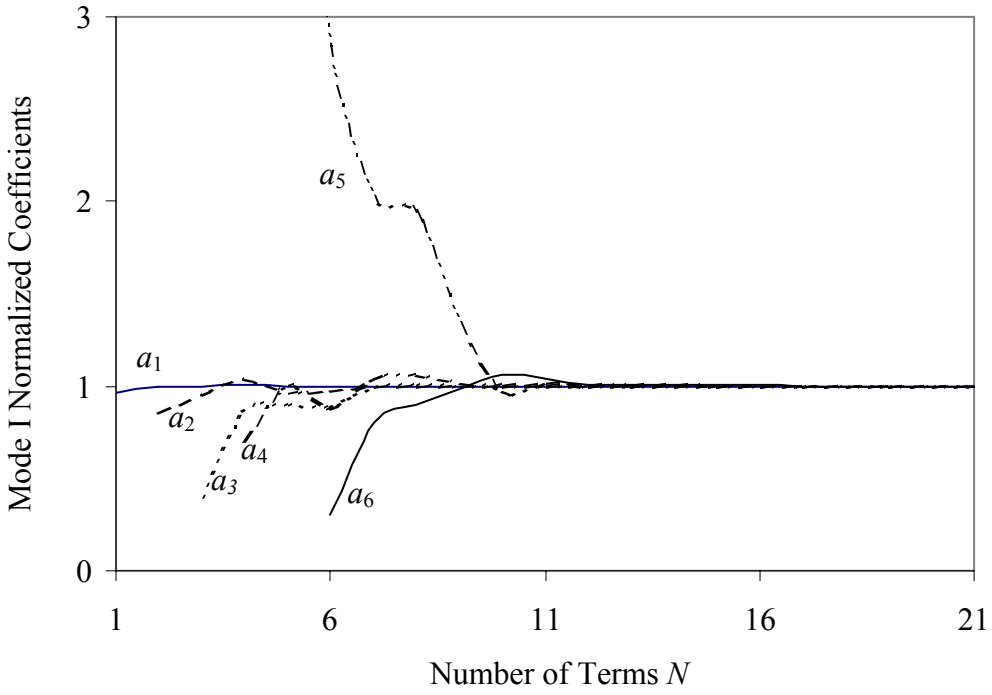

(a) SECT

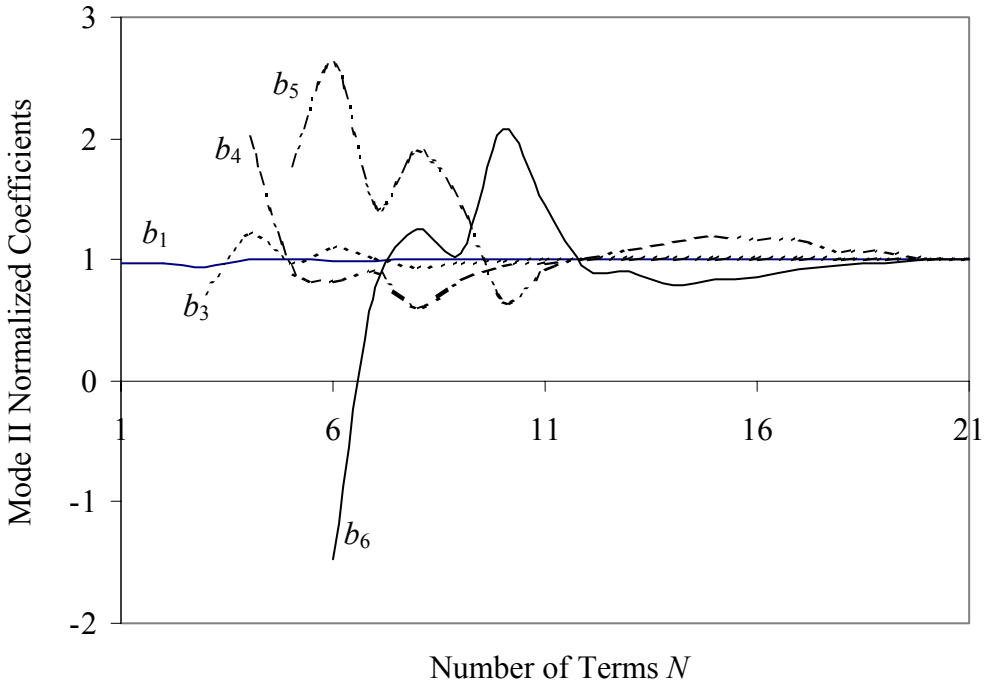

(b) SECS

Fig. 5. Variations of normalized coefficients against number of terms N, (a) SECT and (b) SECS

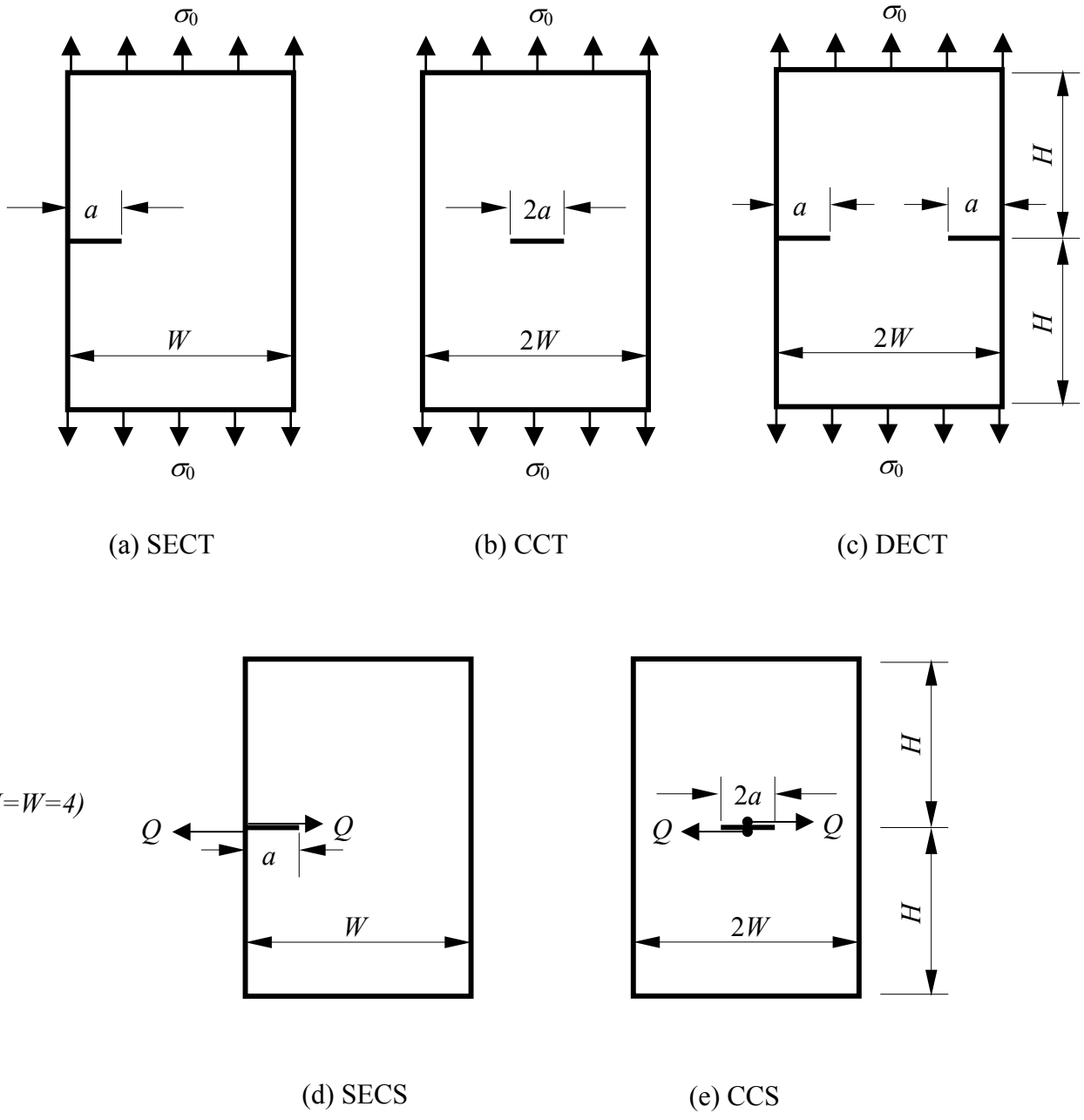

Fig. 6. Example problems for calculation of the higher-degree coefficients: (a) Single Edge Crack Tension (SECT), (b) Centred Crack Tension (CCT), (c) Double Edge Crack Tension (DECT), (d) Single Edge Crack Shear (SECS) and (e) Centred Crack Shear (CCS).